Modulation of bilayer quantum Hall states by tilted-field-induced subband-Landau-level coupling

N. Kumada,[1] K. Iwata,[2] K. Tagashira,[3] Y. Shimoda,[3] K. Muraki,[1] Y. Hirayama,[1,4,*] and A. Sawada[2]
[1]*NTT Basic Research Laboratories, NTT Corporation, 3-1 Morinosato-Wakamiya, Atsugi, Kanagawa 243-0198, Japan*
[2]*Research Center for Low Temperature and Materials Sciences, Kyoto University, Kyoto 606-8502, Japan*
[3]*Department of Physics, Tohoku University, Sendai 980-8578, Japan*
[4]*SORST-JST, 4-1-8 Honmachi, Kawaguchi, Saitama 331-0012, Japan*
(Received 26 September 2007; revised manuscript received 27 February 2008; published 24 April 2008)

We study effects of tilted magnetic fields on energy levels in a double-quantum-well (DQW) system, focusing on the coupling of subbands and Landau levels (LLs). The subband-LL coupling induces anticrossings between LLs directly manifested in the magnetoresistance. The anticrossing gap becomes larger than the spin splitting at the tilting angle $\theta \sim 20°$ and larger than the cyclotron energy at $\theta \sim 50°$, demonstrating that the subband-LL coupling exerts a strong influence on quantum Hall states even at a relatively small θ and plays a dominant role for larger θ. We also find that when the DQW potential is asymmetric, LL coupling occurs even within a subband. Calculations including higher-order coupling reproduce the experimental results quantitatively well.

DOI: 10.1103/PhysRevB.77.155324 PACS number(s): 73.43.−f, 73.21.Fg, 71.70.Di

I. INTRODUCTION

In a two-dimensional electron system (2DES), an in-plane magnetic field $B_\parallel$ that is applied parallel to the 2D plane is used to control and investigate quantum Hall (QH) states. For an ideal 2DES with zero thickness, $B_\parallel$ couples to the system only through the Zeeman energy while the perpendicular magnetic field $B_\perp$ couples with the orbital degree of freedom as well. That is, by tilting the magnetic field away from normal to the 2DES while keeping $B_\perp$ fixed, the Zeeman energy is controlled without changing other energies. This technique was used to elucidate the effects of spins.[1,2] In a bilayer system, which consists of two parallel 2DESs, the importance of $B_\parallel$ increases because $B_\parallel$ changes the tunneling amplitude[3,4] and the relative phase[5,6] between the two layers. The change in the tunneling amplitude, together with the enhancement of the Zeeman energy, is widely used to investigate the ground and excited states of the bilayer QH states.[7,8] The relative phase affects the ground state properties of a coherent bilayer QH state.[9,10]

On the other hand, in a system with more than two occupied spatial subbands, such as quasi-2D heterojunctions[11,12] or parabolic quantum wells,[13–15] coupling of the subbands and Landau levels (LLs) in tilted magnetic fields causes anticrossings between LLs belonging to different subbands. Moreover, since the subband-LL coupling changes the microscopic properties of the wave functions, it affects many-body states, as discussed for a collective mode in the coherent bilayer QH state[16] or $B_\parallel$-induced reorientation of the stripe phase.[17] It is, therefore, important to quantitatively study the coupling in a system with well-defined bilayer potential.

In this work, we carried out transport experiments in tilted magnetic fields by using a double-quantum-well (DQW) sample, in which the potential symmetry can be tuned by gates deposited on the front and back sides of the sample. In a perpendicular field, crossings between LLs belonging to different subbands are manifested by a missing or weakening of the QH states at integer fillings. When the DQW is tilted in the magnetic field, the subband-LL coupling leads to anticrossings. The anticrossing gap increases with tilting angle θ. In a symmetric DWQ, it becomes larger than the Zeeman energy at $\theta \sim 20°$ and larger than the cyclotron energy at $\theta \sim 50°$, so that crossings are avoided between LLs that are not coupled to each other. When the DQW is asymmetric, coupling of LLs in the same subband occurs, modifying the anticrossings and the avoided crossings. We calculated the energy levels from the viewpoint of a single-particle picture and show that they reproduce experiments very well.

This paper is organized as follows: Section II describes a theory by which energy levels in a bilayer system subjected to tilted magnetic fields can be calculated. In Sec. III, we describe the DQW sample and the experimental setup. In Sec. IV, the experimental results are presented and compared to the calculation.

II. THEORETICAL BACKGROUND

In this section, we present a theory describing the effects of an in-plane field on energy levels in a bilayer system. For the moment, we neglect the spin degree of freedom for simplicity. Electrons subjected to a tilted magnetic field $(B_\parallel, 0, B_\perp)$ in a DQW potential $V(z)$ are described by the Hamiltonian

$$H = \frac{\hbar^2 k_x^2}{2m^*} + \frac{e^2 B_\perp^2}{2m^*} x^2 + \frac{\hbar^2 k_z^2}{2m^*} + V(z) + \frac{e^2 B_\parallel^2}{2m^*} z^2 - \frac{e^2 B_\parallel B_\perp}{m^*} xz, \tag{1}$$

where m^* is the effective mass. To obtain Eq. (1), we used the Landau gauge $(0, B_\perp x - B_\parallel z, 0)$ and applied the transformation $x \rightarrow x - \hbar k_y / eB_\perp$. The first four terms describe electrons in a perpendicular magnetic field, where energy levels are LLs in bonding (B) and antibonding (A) subbands. The last two terms of Eq. (1) stem from the in-plane magnetic field. The z^2 term causes a diamagnetic shift, which merely modifies the energies of the bonding and antibonding states. The last term is most important for this work: the cross term

TABLE I. Matrix representation of H. $E_{\perp}^{N,B}=\hbar\omega_{c\perp}(N+\frac{1}{2})-\frac{\Delta_{\mathrm{BAB}}}{2}$ is the eigenenergy of (N,B) in a perpendicular field.

	(N,B)	(N,A)	$(N+1,B)$	$(N+1,A)$
(N,B)	$E_{\perp}^{N,B}+\frac{\hbar\omega_{c\parallel}}{2}\langle B\lvert\frac{z^2}{l_{B\parallel}^2}\rvert B\rangle$	0	$\hbar\omega_{c\perp}\tan\theta\sqrt{\frac{N+1}{2}}\langle B\lvert\frac{z}{l_{B\perp}}\rvert B\rangle$	$\hbar\omega_{c\perp}\tan\theta\sqrt{\frac{N+1}{2}}\langle B\lvert\frac{z}{l_{B\perp}}\rvert A\rangle$
(N,A)	0	$E_{\perp}^{N,A}+\frac{\hbar\omega_{c\parallel}}{2}\langle A\lvert\frac{z^2}{l_{B\parallel}^2}\rvert A\rangle$	$\hbar\omega_{c\perp}\tan\theta\sqrt{\frac{N+1}{2}}\langle A\lvert\frac{z}{l_{B\perp}}\rvert B\rangle$	$\hbar\omega_{c\perp}\tan\theta\sqrt{\frac{N+1}{2}}\langle A\lvert\frac{z}{l_{B\perp}}\rvert A\rangle$
$(N+1,B)$	$\hbar\omega_{c\perp}\tan\theta\sqrt{\frac{N+1}{2}}\langle B\lvert\frac{z}{l_{B\perp}}\rvert B\rangle$	$\hbar\omega_{c\perp}\tan\theta\sqrt{\frac{N+1}{2}}\langle B\lvert\frac{z}{l_{B\perp}}\rvert A\rangle$	$E_{\perp}^{N+1,B}+\frac{\hbar\omega_{c\parallel}}{2}\langle B\lvert\frac{z^2}{l_{B\parallel}^2}\rvert B\rangle$	0
$(N+1,A)$	$\hbar\omega_{c\perp}\tan\theta\sqrt{\frac{N+1}{2}}\langle A\lvert\frac{z}{l_{B\perp}}\rvert B\rangle$	$\hbar\omega_{c\perp}\tan\theta\sqrt{\frac{N+1}{2}}\langle A\lvert\frac{z}{l_{B\perp}}\rvert A\rangle$	0	$E_{\perp}^{N+1,A}+\frac{\hbar\omega_{c\parallel}}{2}\langle A\lvert\frac{z^2}{l_{B\parallel}^2}\rvert A\rangle$

xz couples the subband and Landau quantizations.

The matrix element of H can be expressed, as shown in Table I, by using the eigenstates in a perpendicular field (N,ξ) as a basis set, where N $(=0,1,\ldots)$ and ξ $(=B,A)$ represent the Landau orbit and subband indices, respectively. In a perpendicular magnetic field, the eigenenergy of each basis is

$$E_{\perp}^{N,B(A)}=\hbar\omega_{c\perp}\left(N+\frac{1}{2}\right)-(+)\frac{\Delta_{\mathrm{BAB}}}{2}, \tag{2}$$

where $\omega_{c\perp}$ is the cyclotron frequency due to $B_{\perp}$, Δ_{BAB} is the energy gap between the bonding and antibonding states, which equals the gap between the symmetric and antisymmetric states Δ_{SAS} in a symmetric potential and increases with potential asymmetry. When a finite $B_{\parallel}$ is applied, these diagonal elements undergo a diamagnetic shift of

$$\langle N,\xi\lvert\frac{e^2B_{\parallel}^2}{2m^*}z^2\rvert N,\xi\rangle=\frac{\hbar\omega_{c\parallel}}{2}\langle\xi\lvert\frac{z^2}{l_{B\parallel}^2}\rvert\xi\rangle, \tag{3}$$

where $\omega_{c\parallel}$ and $l_{B\parallel}=\sqrt{\hbar/eB_{\parallel}}$ are the cyclotron frequency and magnetic length associated with $B_{\parallel}$, respectively. More importantly, off-diagonal elements arise from the xz term of Eq. (1). Since $x=(a^{\dagger}+a)/\sqrt{2l_{B\perp}}$ works as the raising $a^{\dagger}$ and lowering a operators of the Landau orbit, it couples LLs when the Landau indices differ by 1, where $l_{B\perp}=\sqrt{\hbar/eB_{\perp}}$ is the magnetic length in $B_{\perp}$. As a result, the matrix element between (N,ξ_i) and $(N+1,\xi_j)$ is

$$\begin{aligned}\langle N,\xi_i\lvert\frac{e^2B_{\parallel}B_{\perp}}{2m^*}xz\rvert N+1,\xi_j\rangle&=\frac{e^2B_{\parallel}B_{\perp}}{m^*}\langle N\lvert\frac{a^{\dagger}+a}{\sqrt{2l_{B\perp}}}\rvert N+1\rangle\langle\xi_i\lvert z\rvert\xi_j\rangle\\&=\hbar\omega_{c\perp}\tan\theta\sqrt{\frac{N+1}{2}}\langle\xi_i\lvert\frac{z}{l_{B\perp}}\rvert\xi_j\rangle,\end{aligned} \tag{4}$$

where $\tan\theta=B_{\parallel}/B_{\perp}$. The spin degree of freedom $(\sigma=\pm1/2)$ can be easily included by adding $\pm\Delta_Z/2$ to the diagonal terms, where Δ_Z is the Zeeman energy.

It is worth mentioning the effects of the symmetry of the confining potential $V(z)$. Figure 1 illustrates the coupling of energy levels in a bilayer system. When $V(z)$ is symmetric, i.e., $V(z)=V(-z)$, B and A correspond to the symmetric and antisymmetric states, respectively. Since z is an antisymmetric function, the intrasubband coupling $\langle\xi_i\lvert z\rvert\xi_i\rangle$ (dotted arrows in Fig. 1) vanishes because of the symmetry, although the intersubband coupling $\langle\xi_i\lvert z\rvert\xi_{j\neq i}\rangle$ (solid arrows in Fig. 1) is finite. This symmetry effect causes a selection rule: LLs in different subbands couple only when the difference between the Landau indices is odd, as shown by the solid arrows in Fig. 1. When $V(z)$ is asymmetric, the intrasubband coupling (dotted arrows in Fig. 1) is nonzero, where the odd/even rule becomes less clear.

To obtain the value of the coupling $\langle\xi_i\lvert z\rvert\xi_j\rangle$ in the DQW sample we used, we calculated the wave functions of the bonding and antibonding states at a total electron density of the two layers $n_t=1.0\times10^{11}$ cm^{-2}; the sample structure is given in Sec. III.

III. EXPERIMENTS

The sample used in this work consists of two 200 Å wide GaAs quantum wells separated by a thin 10 Å-$Al_{0.33}Ga_{0.67}As$ barrier, which was processed into a 50 μm wide Hall bar with Ohmic contacts connecting both layers.[18] Δ_{SAS} decreases from 32 to 23 K when the total density is increased from $n_t=0.7$ to 2.3×10^{11} cm^{-2}. The low-temperature mobility is 1.2×10^6 cm^2/V s with the total electron density of the two layers $n_t=2.0\times10^{11}$ cm^{-2}. The electron densities in the front layer n_f and the back layer n_b are controlled by the front and back-gate biases, respectively. This enables us to independently control the potential symmetry and n_t. Measurements were performed with the sample mounted in the mixing chamber of a dilution refrigerator with a base temperature of 30 mK. By using an *in situ* rota-

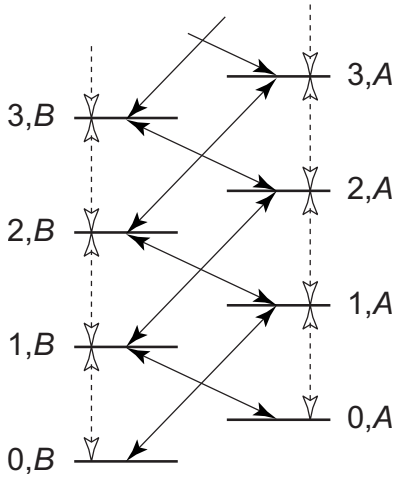

FIG. 1. Schematic overview of the coupling of energy levels in a bilayer system. The solid arrows connect levels coupled by the intersubband-LL coupling. The dotted arrows represent the intrasubband-LL coupling, which operates when the potential is asymmetric.

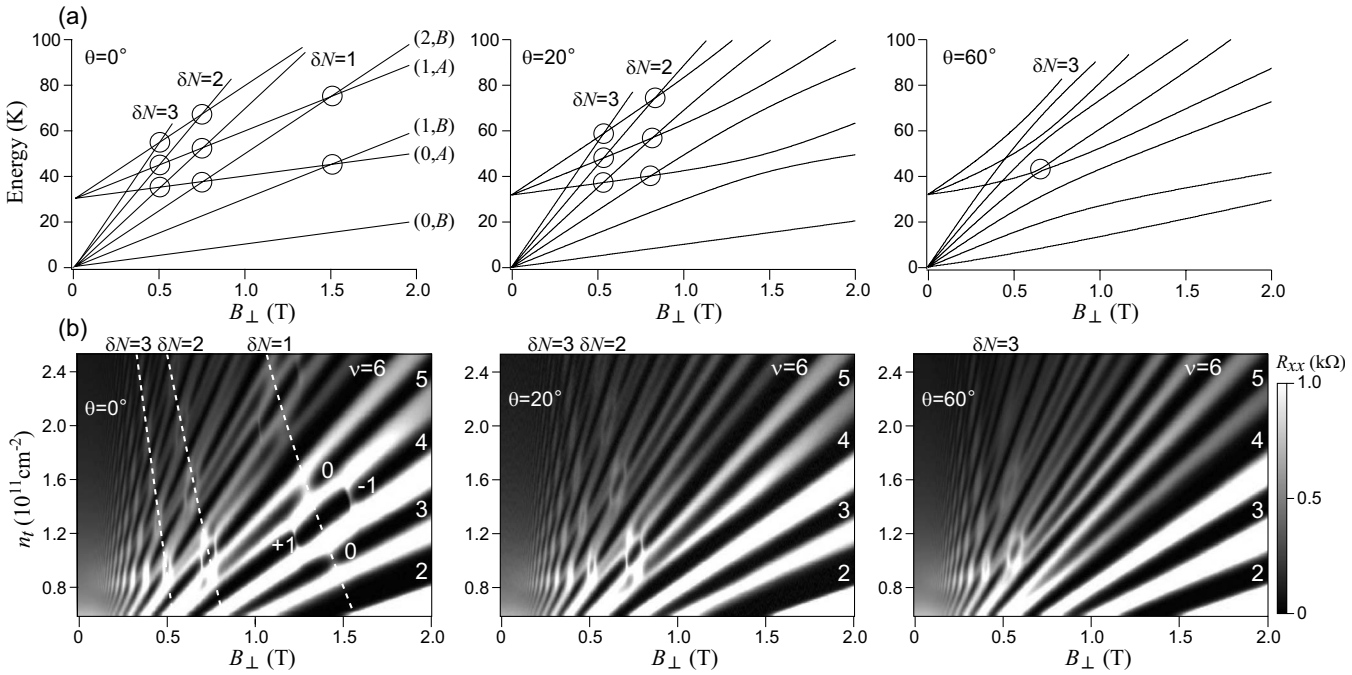

FIG. 2. (a) Calculated energy levels in a symmetric DQW with $\Delta_{SAS}=31.8$ K for tilting angles of $\theta=0°$, 20°, and 60°. Although the energy levels are calculated for $N\leq 12$, levels with higher energies are removed for clarity. The spin splitting is not shown. (b) Gray-scale plots of R_{xx} as a function of the perpendicular field $B_\perp$ and the total density n_t for the three tilting angles. The dark regions represent small values of R_{xx}. In the left panel, $\delta\sigma$ for $\delta N=1$ at $\nu=3-5$ is shown. The dotted lines trace the position of the crossings for $\delta\sigma=0$ at $\delta N=1-3$.

tor, we can tilt the sample in the magnetic field, which has a maximum strength of 13.5 T. Standard low-frequency ac lock-in techniques were used with a current $I=20$ nA.

IV. RESULTS AND DISCUSSION

In this section, we show the experimental data for several tilting angles. The data are compared to the calculated energy levels[19] obtained by solving the matrix in Table I. We are mainly concerned with the results for the case where the DQW is kept symmetric (Sec. IV A). Data for asymmetric DQWs are briefly discussed in Sec. IV B.

A. Symmetric potential

We first show the data for symmetric DQW potentials when n_t is scanned while keeping the densities of the two layers equal ($n_f=n_b$). Figure 2(b) shows the magnetoresistance R_{xx} for three tilting angles as a function of $B_\perp$ and n_t. The dark regions represent small values of R_{xx} and thus QH regions. The left panel presents the data for the perpendicular field ($\theta=0°$), showing two sets of Landau fans originating from the symmetric and antisymmetric subbands with spin splitting. Many LL crossings accompanied by an increase in R_{xx} occur when

$$\delta N\times\hbar\omega_{c\perp}+\delta\sigma\times\Delta_Z=\Delta_{SAS}, \tag{5}$$

where δN is the difference between the Landau indices for crossing levels. Here, $\delta\sigma=0(\pm 1)$ identifies crossings between parallel (antiparallel) spin levels. Note that although N is not a good quantum number in a tilted field, the notation δN is still used for convenience in identifying LL crossings. When the sample is tilted at $\theta=20°$, all LL crossings with $\delta N=1$ [those at $\nu=3-5$ around $B_\perp=1.4$ T and at $\nu=7-9$ around $B_\perp=1.2$ T in Fig. 2(b), left] vanish, as clearly demonstrated in Fig. 2(b), center. At this tilting angle, LL crossings for $\delta N\geq 2$ remain intact. As θ is further increased to $\theta=60°$ [Fig. 2(b), right], the LL crossings for $\delta N=2$ as well as for $\delta N=1$ vanish.

Calculated energy levels based on the subband-LL coupling reproduce the experimental results [Fig. 2(a)]. In the following, the effects of the subband-LL coupling are quantitatively discussed with experimental results for fine increments of θ and calculations.

1. $\delta N=1$

We show the results for small θ ($\leq 20°$), focusing on $\delta N=1$ crossings. Figure 3(b) presents the evolution of QH states around the $\delta N=1$ crossings. In a perpendicular magnetic field, four level crossings with different $\delta\sigma$ occur [Fig. 3(b), left]. Note that the sharp features at $\nu=4$ for $\delta\sigma=\pm 1$ are characteristic of the first-order phase transitions associated with easy-axis ferromagnetism.[18,20] On the other hand, the broad features at $\nu=3$ and 5 for $\delta\sigma=0$ are due to easy-plane ferromagnetism.[18,20] As the sample is tilted $\theta=15°$, the LL crossings for $\delta\sigma=0$ disappear first [Fig. 3(b), center]. At the same time, the magnetic field positions of the two transitions for $\delta\sigma=\pm 1$ approach each other. Further tilting of the sample ($\theta=20°$) causes them to disappear [Fig. 3(b), right]. In Fig. 3(c), activation energy gaps at different mag-

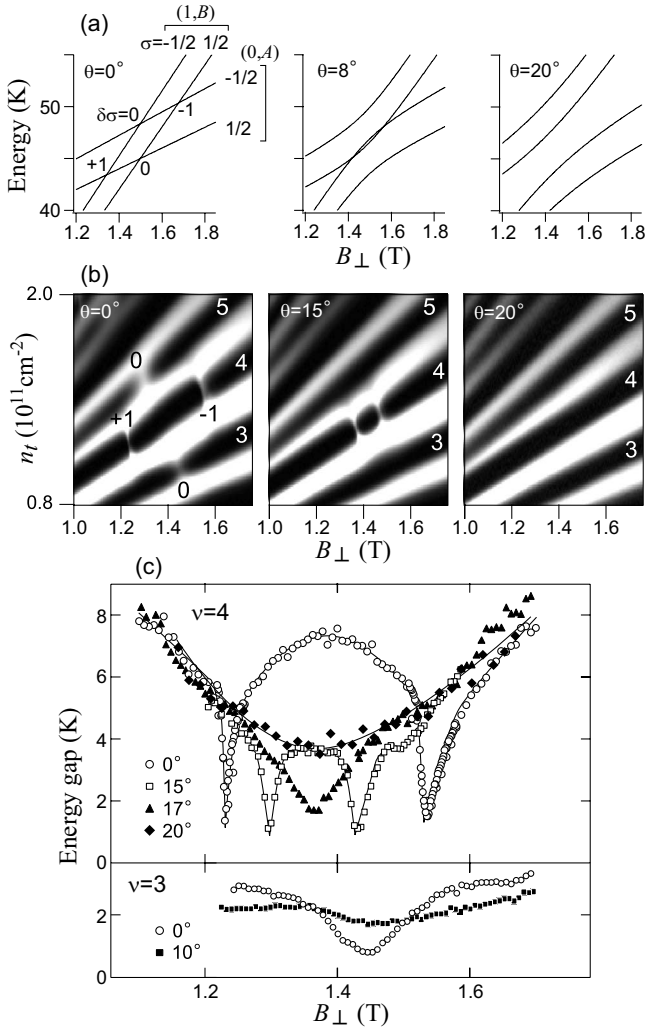

FIG. 3. (a) Calculated energy levels around $\delta N=1$ crossings at $\nu=3-5$ for $\theta=0°$, 8°, and 20°. (b) Gray-scale plots of R_{xx} for $\theta=0°$, 15°, and 20° around $\delta N=1$ crossings at $\nu=3-5$. (c) Activation energy gap as a function of $B_\perp$ for fixed filling factors of $\nu=3$ and 4 for several tilting angles. The lines are guides for the eye.

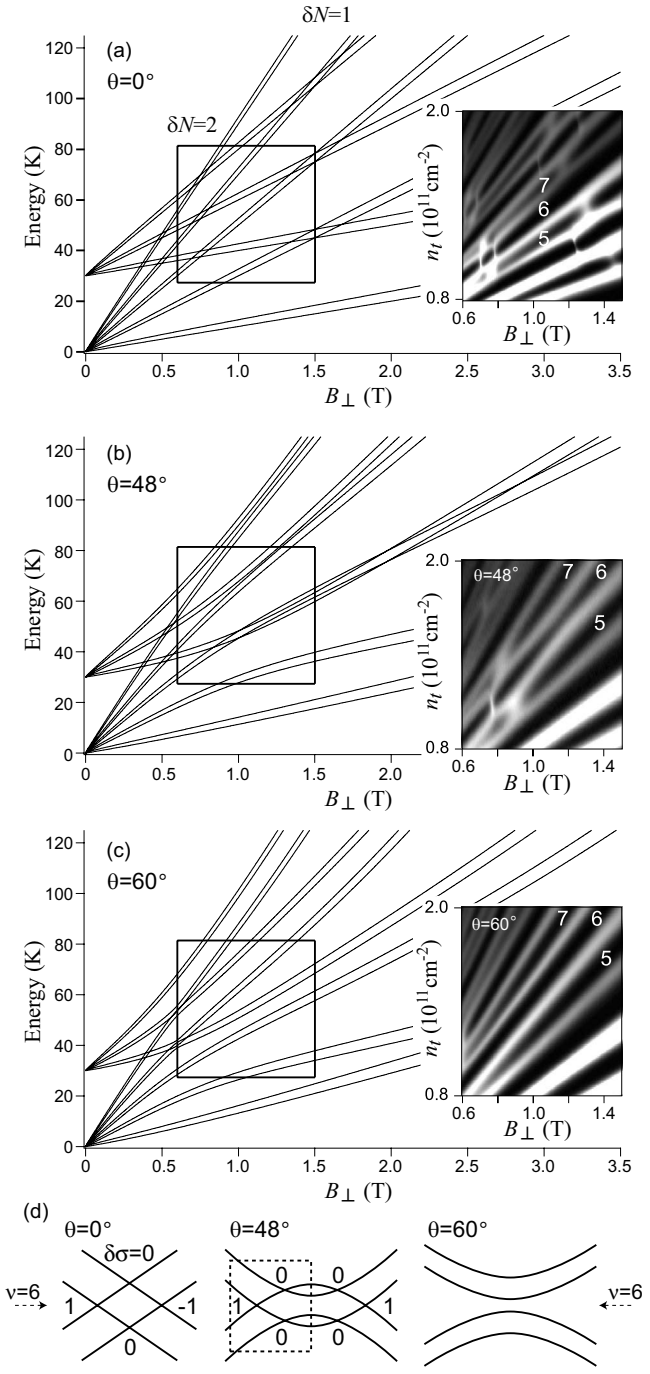

FIG. 4. Calculated energy levels and gray-scale plots of R_{xx} around $\delta N=2$ crossings at $\nu=5-7$ crossings for (a) $\theta=0°$, (b) 48°, and (c) 60°. Experimental regions for the gray-scale plots are indicated by the boxes. (d) Schematic of the evolution of the energy levels. The dotted lines in the center panel indicate the experimental region.

netic fields with fixed filling factors of $\nu=3$ and 4 for several tilting angles are shown, where the activation energy gap Δ is determined from the temperature dependence of $R_{xx} \propto \exp(-\Delta/2T)$. For $\nu=4$, the two sharp minima in Δ first come close to each other ($\theta=15°$) and then merge ($\theta=17°$) before turning into a single broad minimum ($\theta=20°$). For $\nu=3$, Δ becomes almost field independent already at $\theta=10°$.

The experimental results are compared to the calculated energy levels [Fig. 3(a)]. We note that for the calculation, we used enlarged spin splitting $\Delta_Z=g^*\mu_B(B_\perp^2+B_\parallel^2)^{1/2}+2.3B_\perp^{1/2}$, which effectively incorporates the exchange energy; the value of 2.3 is deduced by the level crossing points for $\delta\sigma=\pm 1$. In a tilted field, the like-spin levels $(1,B,\sigma)$ and $(0,A,\sigma)$ couple, which causes the anticrossings between these levels with the gap increasing in proportion to $\tan\theta$ [Eq. (4)]. As a result, an energy gap opens in the QH states at $\nu=3$ and 5 [Fig. 3(a), center, and Fig. 3(c)]. On the other hand, since σ is a good quantum number even in a tilted field, the coupling between levels with opposite spins does not occur. However, as shown in Fig. 3(a), right, the $\delta\sigma=\pm 1$ crossings can be avoided when the anticrossing gap exceeds the spin splitting. We refer to this type of disappearance of the LL crossings as "avoided crossings" to distinguish it from "anticrossings." The overall similarity between Figs. 3(a) and 3(b) clearly shows that the subband-LL cou-

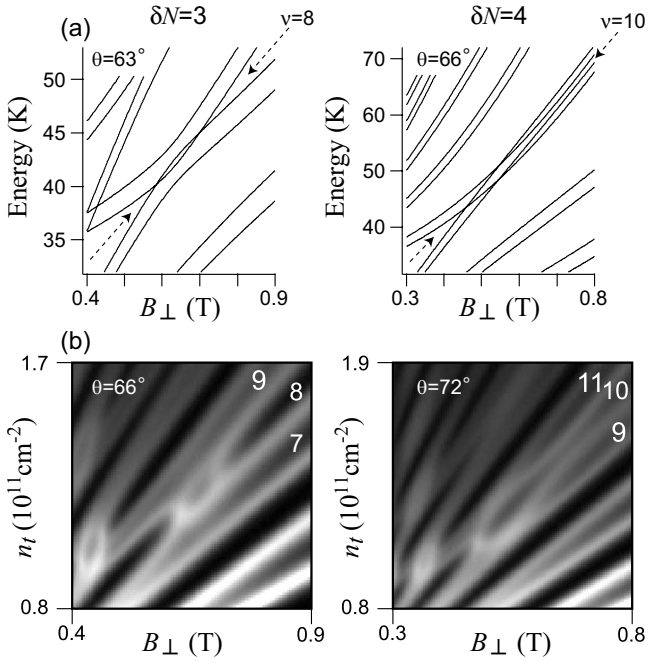

FIG. 5. (a) Calculated energy levels around $\delta N=3$ crossings at $\nu=7-9$ for $\theta=63°$ (left panel) and $\delta N=4$ crossings at $\nu=9-11$ for $\theta=66°$ (right panel). (b) Gray-scale plots of R_{xx} around $\delta N=3$ crossings at $\nu=7-9$ for $\theta=66°$ (left panel) and $\delta N=4$ crossings at $\nu=9-11$ for $\theta=72°$ (right panel).

pling is enough to explain the disappearance of all the LL crossings for $\delta N=1$. These results demonstrate that the subband-LL coupling exerts strong influence on bilayer QH states even at small $B_{\parallel}$, particularly when LLs belonging to different subbands are close to degeneracy.

2. $\delta N=2$

Next, we show the results for larger θ, where LL crossings for $\delta N=2$ disappear. We focus on those occurring at $\nu=5-7$, which are located around $B_{\perp}=0.7$ T at $\theta=0°$ [Fig. 4(a)]. Similar to the data for $\delta N=1$ at $\theta=0°$, there are broad (sharp) features for $\delta\sigma=0$ ($\delta\sigma=\pm 1$) at odd (even) ν. However, the data at $\theta=48°$ show that the behavior of the $\delta N=2$ crossings is different from that of $\delta N=1$ [Fig. 4(b)]. Namely, the $\delta\sigma=-1$ crossing vanishes, leaving the $\delta\sigma=1$ crossing at $B=0.8$ T almost intact. The absence of the anticrossing for $\delta\sigma=0$ at $\nu=5$ and 7 indicates that there is no subband-LL coupling for $\delta N=2$, which is consistent with the symmetry arguments. When the sample is further tilted ($\theta=60°$), all of the crossings for $\delta N=2$ disappear [Fig. 4(c)].

The behavior of $\delta N=2$ crossings can be explained as the avoided crossings caused by the subband-LL coupling for $\delta N=1$, not for $\delta N=2$. When the anticrossing gap for $\delta N=1$ becomes larger than $\hbar\omega_{c\perp}-\Delta_Z$, the $\delta\sigma=-1$ crossing for $\delta N=2$ is avoided, as schematically shown in Fig. 4(d). Subsequently, as the gap exceeds $\hbar\omega_{c\perp}+\Delta_Z$, LL crossings for $\delta\sigma=0$ and 1 are avoided. The calculated energy levels agree with experiments not only on the sequence of the avoidance but also on the field positions of the crossings. These results show that for large θ bilayer QH states are strongly modified

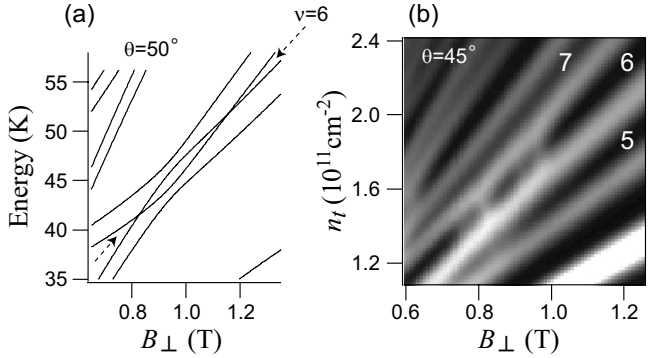

FIG. 6. (a) Calculated energy levels around $\delta N=2$ crossings at $\nu=5-7$ for $\theta=50°$ in the asymmetric potential with $n_f:n_b=2:1$. (b) Gray-scale plot of R_{xx} around $\delta N=2$ crossings at $\nu=5-7$ for $\theta=45°$ in the asymmetric potential.

even though the subband-LL coupling between relevant energy levels does not occur.

3. $\delta N=3$ and 4

We also measured R_{xx} for still larger θ. Figure 5(b) shows a gray-scale plot of R_{xx} around $\delta N=3$ crossings for $\theta=66°$ and that around $\delta N=4$ crossings for $\theta=72°$. The data for $\delta N=3$ and 4 show a behavior similar to that for $\delta N=1$ and 2, respectively. Namely, the disappearance of the crossings for $\delta N=3$ first occurs for $\delta\sigma=0$ at $\nu=7$ and 9, while that for $\delta N=4$ starts from $\delta\sigma=-1$ at $\nu=10$. This is evidence of the anticrossing for $\delta N=3$ at $\sigma=0$ and the avoided crossings for $\delta N=4$, which confirms the higher-order coupling and the resultant odd/even selection rule. The calculation quantitatively explains this behavior well [Fig. 5(a)].

B. Asymmetric potential

Finally, we show the data for an asymmetric DQW, where the ratio of the density in the front layer n_f and the back layer n_b is fixed as $n_f:n_b=2:1$. Figure 6(b) shows a gray-scale plot of R_{xx} around $\delta N=2$ crossings for $\theta=45°$. The disappearance of LL crossings first occurs for $\delta\sigma=0$ at $\nu=5$ and 7. This is contrastive to the data for $\delta N=2$ and 4 in a symmetric potential [Fig. 4(b) and right panel in Fig. 5(b)], where the disappearance of LL crossings first occurs at $\delta\sigma=-1$. This is a clear evidence of the onset of the intrasubband coupling (dotted arrows in Fig. 1) and the resultant anticrossing for $\delta N=$even [Fig. 6(a)]. The existence of the intrasubband coupling indicates that even in a system with only one subband, microscopic properties of wave functions are still affected by $B_{\parallel}$.

V. CONCLUSIONS

In conclusion, we studied effects of tilted magnetic fields on energy levels in a DQW sample by transport measurements and theoretical calculations. When the sample with symmetric DQW potential is tilted in the magnetic field, LLs belonging to different subbands anticross because of the subband-LL coupling. The gap of the anticrossing becomes larger than the spin splitting at $\theta\sim 20°$ and the cyclotron

energy at $\theta \sim 50°$, causing the avoidance of LLs that are not coupled to each other. We also carried out experiments in an asymmetric DWQ, showing that the potential symmetry modifies the subband-LL coupling. The calculated energy levels quantitatively reproduce the experimental results well. We suggest that since the subband-LL coupling modifies microscopic properties of wave functions, it affects many-body states even in single-layer systems.

ACKNOWLEDGMENT

The authors are grateful to T. Saku for growing the heterostructures.

APPENDIX

In the main body of this paper, we presented the calculated energy levels as a function of $B_\perp$ with fixed θ to compare to the experimental results. To more directly illustrate the effects of the tilted field on the energy levels in this appendix, we showed the energy levels as a function of θ with fixed $B_\perp$. Figure 7(a) depicts the results for a symmetric DQW potential. Compared to the previous theory,[3] we chose $B_\perp = 2$ T, where $\hbar\omega_{c\perp}$ (=40 K) is slightly larger than Δ_{SAS} (=31.8 K). In the calculated range $(0° \leq \theta \leq 83°)$, Δ_Z ($\leq$8.4 K) is much smaller than $\hbar\omega_{c\perp}$ and Δ_{SAS}, and we set $\Delta_Z = 0$ in the following discussion for simplicity. Then, at $\theta = 0°$, the energy gaps at $\nu = 4N+2$ and $4N+4$ are given by Δ_{SAS} and $\hbar\omega_{c\perp} - \Delta_{\mathrm{SAS}}$, respectively. As Fig. 7(a) shows, when the magnetic field is tilted away from $\theta = 0°$, the intersubband-LL coupling between the adjacent orbital levels, (N,A) and $(N+1,B)$, increases the gap at $\nu = 4N+4$, which in turn decreases the gaps at $\nu = 4N+2$. As θ is increased, the energy gap at $\nu = 4N+2$ goes to zero and then becomes finite again for $N \geq 1$. Such a behavior results from the crossings between the energy levels composed of (N,B) and $(N-1,A)$ and composed of $(N+1,B)$ and (N,A), which do not couple with each other due to the absence of the intrasubband-LL coupling (Fig. 1). By increasing θ further, the intersubband-LL coupling of higher orders causes oscillations of the energy levels, which leads to the repeated oscillations of the $\nu = 4N+2$ gap across zero for $N \geq 2$. All these calculations are in accordance with the theory in Ref. 3 if the $\nu = 4N+2$ gap is associated with the tunneling gap for the Nth Landau level,[22] which is also consistent with the recently observed reentrant QH states.[21]

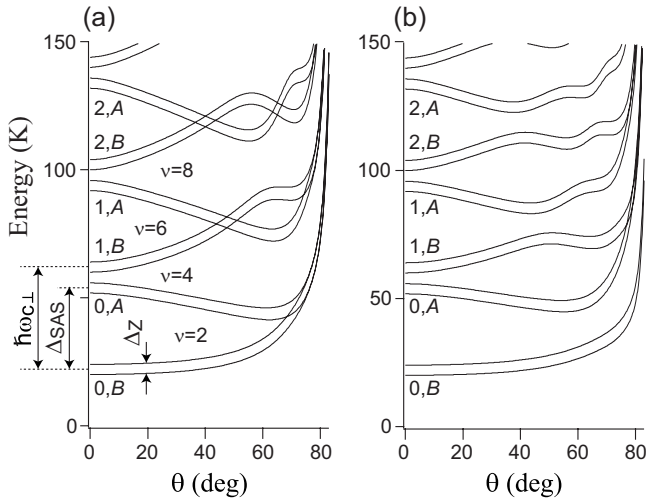

FIG. 7. Calculated energy levels as a function of θ in (a) the symmetric DQW potential and (b) the asymmetric DQW potential with $n_f : n_b = 2:1$. $\Delta_{\mathrm{SAS}} = 31.8$ K and $B_\perp = 2.0$ T are fixed. N and ξ for each level at $\theta = 0°$ are shown. The overall shift to higher energies at very large θ is due to the diamagnetic shift.

In Ref. 3, they take the wave functions localized in each layer, which are subjected to a tilted field, as a basis set and analytically evaluate the interlayer hopping probability by using a zero-QW-thickness approximation. On the other hand, we take as a basis set the bonding and antibonding states and numerically calculate the energy levels in a tilted field. While these two approaches are essentially the same, one obvious advantage of our method is that it can deal with DQWs with an arbitrary potential, including the asymmetric ones. As shown in Fig. 7(b), when the DQW potential is made asymmetric, the intrasubband-LL coupling becomes finite and the energy gaps open throughout. Thus, our calculations can shed light on the important roles of potential asymmetry, which have not been considered in previous studies.

*Present address: Department of Physics, Tohoku University, Sendai 980-8578, Japan.

[1] J. P. Eisenstein, H. L. Störmer, L. N. Pfeiffer, and K. W. West, Phys. Rev. B **41**, 7910 (1990).

[2] A. Schmeller, J. P. Eisenstein, L. N. Pfeiffer, and K. W. West, Phys. Rev. Lett. **75**, 4290 (1995).

[3] J. Hu and A. H. MacDonald, Phys. Rev. B **46**, 12554 (1992).

[4] R. Côté, H. A. Fertig, J. Bourassa, and D. Bouchiha, Phys. Rev. B **66**, 205315 (2002).

[5] K. Yang, K. Moon, L. Zheng, A. H. MacDonald, S. M. Girvin, D. Yoshioka, and S. C. Zhang, Phys. Rev. Lett. **72**, 732 (1994).

[6] C. B. Hanna, A. H. MacDonald, and S. M. Girvin, Phys. Rev. B **63**, 125305 (2001).

[7] T. S. Lay, T. Jungwirth, L. Smrčka, and M. Shayegan, Phys. Rev. B **56**, R7092 (1997).

[8] N. Kumada, D. Terasawa, Y. Shimoda, H. Azuhata, A. Sawada, Z. F. Ezawa, K. Muraki, T. Saku, and Y. Hirayama, Phys. Rev. Lett. **89**, 116802 (2002).

[9] S. Q. Murphy, J. P. Eisenstein, G. S. Boebinger, L. N. Pfeiffer, and K. W. West, Phys. Rev. Lett. **72**, 728 (1994).

[10] Z. F. Ezawa, *Quantum Hall Effects: Field Theoretical Approach and Related Topics* (World Scientific, Singapore, 2000).

[11] Z. Schlesinger, J. C. M. Hwang, and S. J. Allen, Phys. Rev. Lett. **50**, 2098 (1983).

[12] A. D. Wieck, F. Thiele, U. Merkt, K. Ploog, G. Weimann, and W. Schlapp, Phys. Rev. B **39**, 3785 (1989).

[13] K. Ensslin, C. Pistitsch, A. Wixforth, M. Sundaram, P. F. Hopkins, and A. C. Gossard, Phys. Rev. B **45**, 11407 (1992).
[14] G. M. Gusev, A. A. Quivy, T. E. Lamas, J. R. Leite, O. Estibals, and J. C. Portal, Phys. Rev. B **67**, 155313 (2003).
[15] G. Yu, D. J. Lockwood, A. J. SpringThorpe, and D. G. Austing, Phys. Rev. B **76**, 085331 (2007).
[16] Y. Yu, Phys. Rev. B **66**, 113309 (2002).
[17] T. Jungwirth, A. H. MacDonald, L. Smrčka, and S. M. Girvin, Phys. Rev. B **60**, 15574 (1999).
[18] K. Muraki, T. Saku, and Y. Hirayama, Physica E (Amsterdam) **12**, 8 (2002).
[19] For the calculation, Δ_{SAS} is fixed to 31.8 K, which corresponds to the value at $n_t=1.0\times10^{11}$ cm^{-2}. We calculate levels for $N\leq12$; we confirmed that in the region of our concern, results remain almost unchanged as the number of levels included is increased.
[20] K. Muraki, T. Saku, and Y. Hirayama, Phys. Rev. Lett. **87**, 196801 (2001).
[21] G. M. Gusev, A. K. Bakarov, T. E. Lamas, and J. C. Portal, Phys. Rev. Lett. **99**, 126804 (2007).
[22] The interpretation that the $\nu=4N+2$ gap corresponds to the tunneling gap for the Nth Landau level, however, is invalid for most of the experimental condition used in the present study, where $\Delta_{\mathrm{SAS}}>\hbar\omega_{c\perp}$.